Oxide-diluted magnetic semiconductors: a review of the experimental status

2003 J. Phys.: Condens. Matter 15 R1583

(http://iopscience.iop.org/0953-8984/15/37/R01)

INSTITUTE OF PHYSICS PUBLISHING JOURNAL OF PHYSICS: CONDENSED MATTER

J. Phys.: Condens. Matter **15** (2003) R1583–R1601 PII: S0953-8984(03)66055-8

TOPICAL REVIEW

Oxide-diluted magnetic semiconductors: a review of the experimental status

W Prellier, A Fouchet and B Mercey

Laboratoire CRISMAT, CNRS UMR 6508, ENSICAEN, 6 Boulevard du Maréchal Juin, F-14050 Caen Cedex, France

E-mail: prellier@ismra.fr

Received 10 July 2003
Published 8 September 2003
Online at stacks.iop.org/JPhysCM/15/R1583

Abstract

Oxide-diluted magnetic semiconductors (O-DMS) have attracted a great deal of interest in recent years due to the possibility of inducing room temperature ferromagnetism. These materials are of particular interest for spintronic devices such as spin valves. This review describes the experimental status of the O-DMS including the recent results on ZnO- and TiO_2-based systems.

Contents

1. Introduction 1583
2. ZnO-based materials: $Zn_{1-x}M_xO$ (M = Co, Mn, V, Fe. . .) 1585
   2.1. The growth conditions 1585
   2.2. The properties 1586
3. TiO_2-based materials (rutile and anatase) 1589
   3.1. Introduction 1589
   3.2. The growth of Co:TiO_2 thin films 1590
   3.3. The physical properties of Co:TiO_2 thin films 1593
4. Some other host matrix: rutile and perovskite types 1595
   4.1. Rutile-type structures: SnO_2 1595
   4.2. Perovskite-type structures: $ATiO_3$ (A = Ba, Sr, La) 1597
   4.3. Other structures: the example of Cu_2O 1598
5. Conclusion 1599
   Acknowledgments 1599
   References 1599

1. Introduction

In semiconductor devices, one usually takes advantage of the charge of electrons. In contrast, magnetic materials are utilized on the basis of electron spin. In order to develop new electronics,

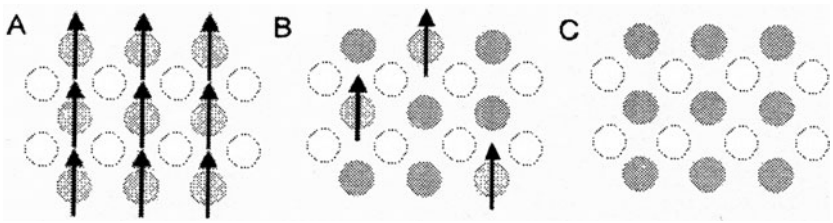

Figure 1. The different types of semiconductors: (A) a magnetic semiconductor; (B) a DMS and (C) a non-magnetic semiconductor.

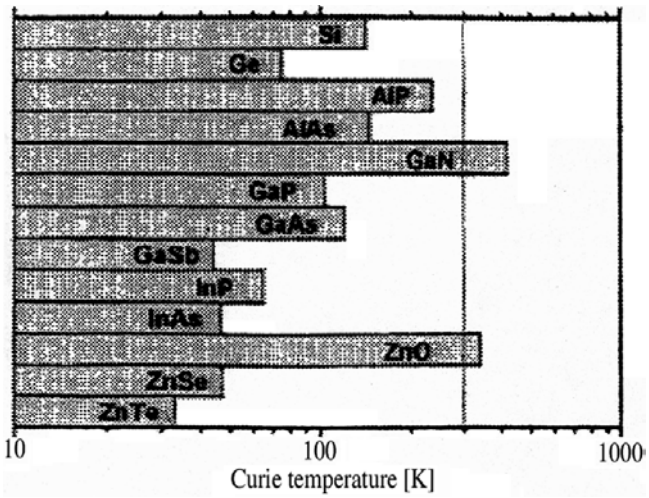

Figure 2. Computed values of Curie temperature for various p-type semiconductors containing 5% of Mn and 3.5×10^{20} hole cm^{-3} (from [6]).

it is interesting to combine both features: the charges and the spins of electrons. In this, the spin of electrons that carries the information can be used as an added degree of freedom in novel electronic devices. Thus, the development of functional ferromagnetic semiconductors is a key to the development of spintronics (or spin-based electronics) [1] that will certainly be the devices utilized in the future.

A variety of semiconductor materials, called diluted magnetic semiconductors (DMS) [2], combine the two interesting properties: semiconducting and magnetic. Such a compound (figure 1(b)) is an alloy between a non-magnetic semiconductor (figure 1(c)) and a magnetic element. Many DMS of III–V (GaAs) or II–VI (CdTe) types have been obtained by doping semiconductors with magnetic impurities (Mn, for example) but most of them have a low Curie temperature (T_C) which limited their interest [3]. In fact, recent first-principles calculations [4] show that the ferromagnetic state of GaN is stable for various doping elements, including V, Cr or Mn, without any additional carrier doping treatments. But, in the end, very few semiconductors exhibiting a high Curie temperature [5] were discovered and the investigation for room temperature DMS, needed for practical applications, was still necessary.

A theoretical prediction by Dietl *et al* [6][1] demonstrates that the Curie temperature can be increased above room temperature in p-type semiconductor-based DMS (see figure 2).

[1] The model is based on consideration of ferromagnetic correlation mediated by holes originating from shallow acceptors in the ensemble of localized spins in doped magnetic semiconductors.

The calculations also show that ferromagnetism (FM) is stable in a DMS which is based on a wide bandgap semiconductor. In addition to that, FM of ZnO-based semiconductors was investigated by *ab initio* calculations based on the local density approximation [7]. These theoretical studies were the first step to oxide-diluted magnetic semiconductors (O-DMS) and several groups started to work in this field. The report of room temperature FM in Co:TiO_2 oxide films [8] has obviously encouraged experimental studies and intensive experimental work has begun in the condensed matter community on O-DMS. Significant efforts were made to grow these oxides, which is possible in a thin film form due to the non-equilibrium process of the techniques used, and various systems with different properties (for example, Curie temperatures) have been obtained.

Here, we present a brief review of the experimental work done over the last four years. This review is divided into three parts which correspond to the three major systems that have been studied. First, we will present the results on the ZnO matrix. In this section, we will focus on the growth conditions and the properties of ZnO wurtzite and their influence with the various dopants. The elements Co and Mn have been mostly used but the effect of doping with V, Fe and Cu will also be presented. In a second section, we will describe the Co-doped TiO_2 (anatase or rutile) phase. In particular, we will discuss the origin of room temperature FM in this system and the controversy coming from the existence of cobalt clusters. Finally, some other mother systems (rutile and perovskite phases) will be presented.

2. ZnO-based materials: $Zn_{1-x}M_xO$ (M = Co, Mn, V, Fe. . .)

ZnO is a II–VI compound semiconductor with a wide bandgap energy ($E_g = 3.35$ eV) and is interesting from the viewpoint of forming a transparent ferromagnetic material. ZnO crystallizes in the wurtzite structure (hexagonal, with $a = 3.25$ Å and $c = 5.12$ Å) [9]. Also, it has electron (n-type) conductivity naturally but p-type conductivity can also be induced by using a co-doping technique [10].

2.1. The growth conditions

2.1.1. Introduction to $Zn_{1-x}M_xO$ compounds (M = transition metal elements). Theoretical work on ZnO system done by Sato and Katayama-Yoshida [7] showed, using first-principles calculations, that doping by 3d transition metal atoms, such as V, Cr, Fe, Co and Ni, in the ZnO matrix exhibits a ferromagnetic ordering without any additional carrier doping while Ti and Cu result in a paramagnetic state. In the case of Mn doping, the calculations show a ferromagnetic state is induced by hole doping. Keeping in mind that highly conductive p-type ZnO can be obtained by the co-doping method [10], the theoretical predictions have opened the route for experimentalists. Soon after, several doping elements (essentially 3d transition elements) have been used, including Mg [11, 12], Ni [13, 14], S [15], V [16], Mn [14, 17–22], Cr [14, 22], Fe [22, 23] and also Co [14, 22, 24–31].

2.1.2. The synthesis. As already said, many studies were done on Co:ZnO films which were deposited either by radio-frequency magnetron co-sputtering [29], pulsed laser deposition (PLD) using a KrF laser [24, 26–28, 30] or a sol–gel method [31]. Due to the wurtzite (hexagonal) structure of ZnO, which is conserved upon doping [14, 24], the substrates used are sapphire (0001)-oriented corresponding to the lower mismatch between the film and the substrate (2%). The films are grown using a ceramic target made by a standard solid-state reaction technique (ZnO and CoO are mixed together, calcined at 500 °C for 7 h and sintered at 950 °C for 12 h in air [30]) but it is also possible to synthesize the films starting from pure metal

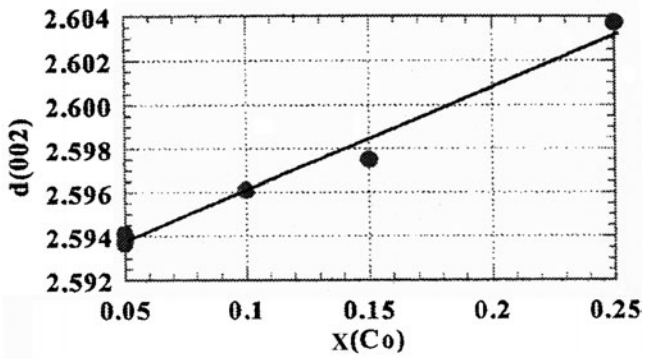

Figure 3. Co content (x) dependence of c-axis lattice constants (d_{002} value) in $Zn_{1-x}Co_xO$ films grown on Al_2O_3 (from [14]).

targets of Zn and Co [24] or two oxide targets (this technique is called alternating deposition, AD) of ZnO and $Zn_{1-x}Co_xO$ [28]. This method allows a homogeneous films' repartition of the Co inside the structure and precise control of the Co content [24, 28] but this also seems possible using a sol–gel process [31]. But more importantly the AD method showed a better crystallinity than conventional methods [28]. The typical deposition conditions of laser ablated films are a temperature of $\leqslant 600\,^{\circ}C$, a partial pressure of oxygen close to 10^{-5}–5×10^{-5} Torr [14, 26, 28, 30] and a laser energy [14, 22, 26, 30] of 1–3 J cm^{-2}. The films are sensitive to the deposition conditions, as observed previously for many oxides. In fact, when the deposition temperature is relatively low ($<600\,^{\circ}C$), homogeneous alloy (predominantly paramagnetic) films with a wurtzite ZnO structure are grown, whereas inhomogeneous films of a wurtzite ZnO phase mixed with rock-salt CoO and hexagonal Co phases form when the temperature is relatively high and the oxygen pressure is fairly low ($<10^{-5}$ Torr) [30].

2.1.3. Solubility of the dopant. The obtained films are single phase with a c-axis orientation, i.e. with the c axis normal to the substrate plane [14]. The Co content dependence of the c-axis lattice constants is shown in figure 3. The d_{002} (equal to $c/2$) value increased linearly as the Co concentration increased, which indicates that the Co ions are systematically substituted for the Zn ions in the film without changing the wurtzite structure (ZnO has the wurtzite structure) [14, 24, 31, 32]. The linear dependence indicates that the values tend to obey the Vergard law at least up to the solubility limit. Surprisingly, various values of the dopant solubility were obtained. For example, Prellier *et al* [24] observed a plateau in the plot of the out-of-plane lattice parameter versus Co content above 10% of the Co content whereas Ueda *et al* [14] clearly observed phase separations into the ZnO and CoO in the film prepared using $Zn_{0.5}Co_{0.5}O$ targets (indicating that the limit is lower than 50%) and Lee *et al* [31] found some undefined peaks for a cobalt content greater than 25%. Kim *et al* [26] claimed that the limit is 40%, close to a previous report [14]. This difference should be attributed to the process which allows a different distribution of the Co inside the ZnO wurtzite structure. Other dopants, such as Ni, can also be dissolved up to 25 at.% in the ZnO structure by a low growth technique [13, 14]. The high solubility of dopants seems to result from the growth conditions. For example, several authors claimed that the non-equilibrium nature of the laser–material interaction allows us to dope at high Mn content (up to 36%) [17, 20, 21]. A series of $Mg_{1-x}Zn_xO$ ($x = 0$, 0.05, 0.1 and 0.15) were also grown by metal–organic chemical vapour deposition [12] and other 3d transition metals, such as Cr [14, 22] or V [16], have been employed.

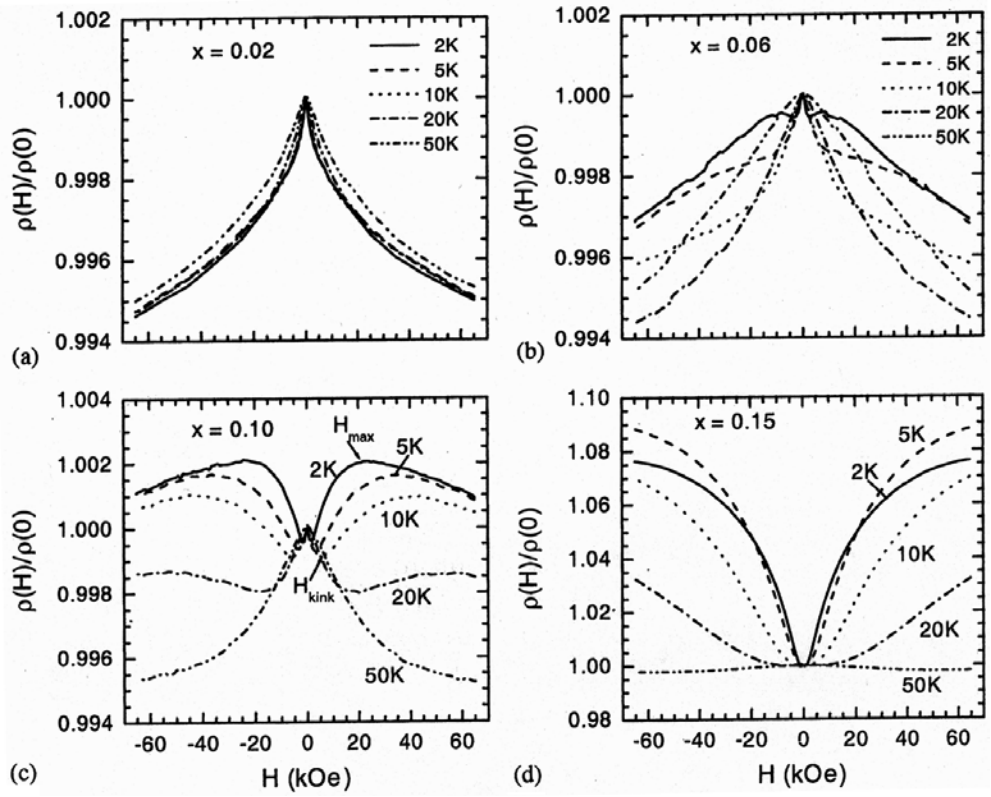

Figure 4. $M(T)$ of the Co:ZnO films (5% of Co) recorded below 2000 G. The inset depicts the $M(H)$ at 30 and 350 K. The 350 K signal is due to the background component of the substrate. The anomaly at 30 K $\pm$ 7000 G corresponds to the difficulty in fitting the signal when crosses zero (from [24]).

2.2. The properties

2.2.1. Magnetization. Regarding the magnetic properties of the Co:ZnO films, many behaviours were obtained by different research groups. Also, the results are not very reproducible. This controversy between research teams may result from the growth method used and/or from the growth conditions (oxygen pressure, deposition temperature, etc). Using the PLD technique, some authors reported FM above room temperature [14, 24], while Jin *et al* [22] found no indication of FM for films grown by utilizing laser molecular beam epitaxy (MBE). Figure 4 shows the magnetization (M) as a function of temperature (T) recorded for a 5% Co-doped ZnO film. The ferromagnetic behaviour is observed from the $M(H)$ over the whole temperature range between 5 and 300 K (see the inset of figure 4) but the hysteresis of the magnetization is very small (a coercivity of a few gauss) [22, 24]. $M(T)$ curves (figure 4) clearly show that the film is ferromagnetic with a Curie temperature (T_C) around 300 K. The transition from the ferromagnetic state to the paramagnetic state is clearly seen, suggesting that the metallic Co clusters (the T_C of the metal Co clusters is 1404 K) are not responsible for the effect observed at 300 K. Moreover, the saturation moment (0.7 μ_B/mol Co for 8% Co-doped film) is lower compared to 1.7 μ_B/mol Co of metallic Co[0], suggesting that the Co state should be close to Co^{2+}. Note that the increase of the out-of-plane lattice parameter as

the cobalt content increases is also in favour of Co^{2+} [24] and that FM at room temperature was also observed with 25% Co with a clear out-of-plane anisotropy [25]. A large amount of work was done using Co as a dopant but Mn has also been used.

A Curie temperature of 70 K was found for $Zn_{0.93}Mn_{0.07}O$ films grown on $(0001)Al_2O_3$ by RF magnetron sputtering [19] whereas no ferromagnetic ordering has been observed at 5 K on films deposited on $(11\bar{2}0)Al_2O_3$ [18]. In addition, the Curie temperature obtained from the temperature-dependent magnetization curves was 30 and 45 K for $Zn_{1-x}Mn_xO$ films deposited on $(0001)Al_2O_3$ with $x = 0.1$ and 0.3, respectively [21]. Up to know, it seems that there are disagreements on the characteristics of the Mn-doped ZnO films. The difference may arise either from the substrate or the growth process. More experiments are required.

Based on theoretical predictions, V was also tried [7] and some results are discussed hereafter. The field dependence of the magnetization curve of $Zn_{0.85}V_{0.15}O$ films measured at 300 K showed a hysteresis loop, indicating a high Curie temperature, with a coercive field of 200 Oe. The saturation magnetization (M_S) of the film is estimated to be 0.5 μ_B/V site from the magnetization versus magnetic field (H) curve at 300 K. These magnetization curves indicate that the films possessed ferromagnetic characteristics. The vanadium concentration dependence of the $M(H)$ curve also showed a hysteresis shape. The $Zn_{0.90}V_{0.10}O$ and $Zn_{0.95}V_{0.05}O$ films also showed ferromagnetic behaviours. The saturation magnetization value of each film seems to depend on the vanadium concentration from 5 to 15%, indicating that the FM becomes more stable as the concentration of vanadium increases [16].

A transition temperature as high as 550 K was obtained in bulk $Zn_{0.94}Fe_{0.05}Cu_{0.01}O$ and the saturation magnetization at room temperature reached a value of 0.75 μ_B/Fe [23]. FM was also observed for the CoFe-doped ZnO films. In this case, a rapid thermal annealing leads to a remarkable increase in the spontaneous magnetization of the films as well as the electron concentration. The annealing also leads to a significant increase in the Curie temperature, resulting in room temperature FM [33].

2.2.2. Magnetotransport properties. It is well known that one of the representative features of DMSs is the giant magnetoresistance [MR = $(R(H) - R(0))/R(0)$] [2]. Figure 5 shows the isothermal MR of $Zn_{1-x}Co_xO$:Al thin films for $x = 0.02$, 0.06, 0.10 and 0.15 at various temperatures (in this case, Al is used to make the films conductive). Three different types of MR behaviour at low temperature (<20 K) are observed, depending on the Co content x: (i) showing only negative MR (figure 5(a), $x = 0.02$), (ii) showing only positive MR (figure 5(d), $x = 0.15$) and (iii) showing a negative MR in weak $H < H_{kink}$ and then a positive MR up to H_{max}, followed by a negative MR above H_{max} (figure 5(c), $x = 0.10$). The MR behaviour for $x = 0.06$ (figure 5(b)) is essentially the same for $x = 0.10$ at low temperatures. As is clearly seen in figure 5(c), the magnetic field H_{kink} at which there occurs an upturn of the resistivity decreases with decreasing temperature at 220 K. The magnetic field H_{max} at which the positive MR shows its maximum peak also decreases with decreasing temperature. All samples exhibit a very small negative MR at high temperature above 50 K, as observed in a ZnO:Al film without magnetic impurity [26].

A large positive MR (60% at 5 K under 2 T) was also observed in $Zn_{0.94}Fe_{0.05}Cu_{0.01}O$ below 100 K [23]. Despite non-magnetic elements, a large MR amount of 26% was observed at 3 K in ZnO:S films [15].

Films show a semiconducting-like behaviour and co-doping with Al in Co:ZnO films results in n-type material [17]. The carrier (electron) concentration was estimated to be 9.2×10^{20} cm^{-3} by Hall measurements for $Zn_{0.98}Co_{0.02}O$:Al (1 mol% of Al) [26]. The carrier concentration is estimated to be 1.2×10^{18} and 2.9×10^{18} cm^{-3} and the mobility is 53.2 and 17.9 for $Zn_{0.75}Co_{0.25}O$ and $Zn_{0.85}Co_{0.15}O$ by the Hall measurements, respectively. The samples

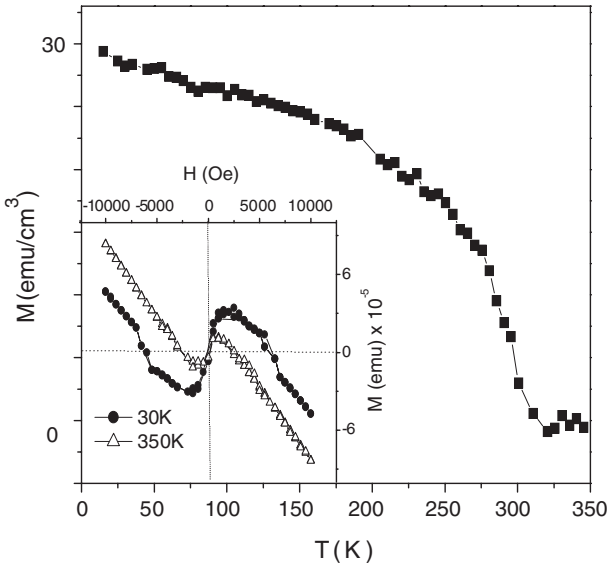

Figure 5. Isothermal MR of laser-deposited $Zn_{1-x}Co_xO$:Al (1 mol% of Al) thin films for $x = 0.02$, 0.06, 0.10 and 0.15 at various temperatures. The magnetic field is applied normal to the film surface (from [26]).

with higher carrier concentration ($Zn_{0.85}Co_{0.15}O$ film) show ferromagnetic characteristics with higher Curie temperature and magnetization saturation, as well as metallic features [14].

In the case of Ni-doped ZnO [13], films with Ni content ranging from 3 to 25 at.% exhibit FM at 2 K but a superparamagnetic behaviour is observed between 30 and 300 K.

2.2.3. Optical properties. The strong magneto-optical effect of $Zn_{1-x}Co_xO$ near the optical bandgap is reported [34]. Magnetic circular dichroism (MCD) and Faraday rotation of $Zn_{1-x}Co_xO$ ($x = 0.012$ and 0.016) at 5 K are as high as 2° cm^{-1} Oe^{-1} at 3.4 eV, which are about two orders larger than those of ZnO. Absence of a strong Co^{2+} dd* transition near the optical bandgap makes $Zn_{1-x}Co_xO$ a useful material for short-wavelength magneto-optical applications. Large magneto-optical effects and paramagnetic temperature dependence of MCD show a strong mixing of the sp bands of the host ZnO with Co^{2+} d orbitals. The polarity of the MCD peak is negative, indicating the antiferromagnetic pd exchange interaction.

The optical properties of the samples were measured by spectroscopic ellipsometry at room temperature in the 1.55 eV photon energy region. As x increases, the optical bandgap absorption edge (E_0) of the alloys shows a redshift from that of pure ZnO, reaching 350 meV for $x = 0.22$. The excitonic character of the E_0 edge is gradually reduced as x increases and is replaced by the three-dimensional critical-point shape. Optical absorption structures are also observed below the E_0 edge near 2 eV and interpreted as due to the transitions between the crystal-field-split 3d levels of tetrahedral Co^{2+} ions substituting for Zn^{2+} ions [32].

The transmittance spectra showed the increase of both the absorption band intensity and the redshift of the absorption peak as well as the band edge with increasing x. Note that these changes depend on Co concentration. These optical properties suggest that spd exchange interactions and typical dd transitions become activated with increasing x, which leads to the enhancement of ferromagnetic properties in $Zn_{1-x}Co_xO$ films as shown in the AGM results. Therefore, it is concluded that the FM derives from the substitution of Co^{2+} for Zn^{2+} without changing the wurtzite structure [29].

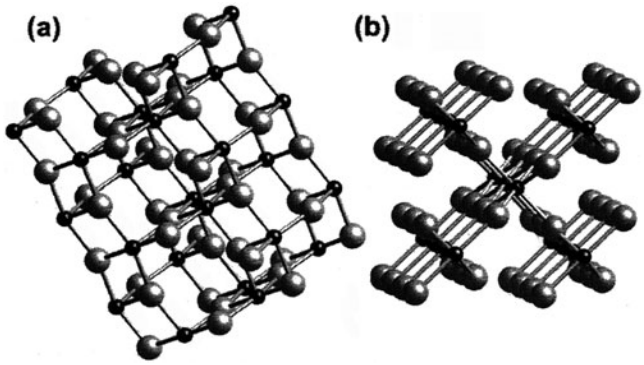

Figure 6. Schematic diagrams of the most stable phases of TiO_2: (a) anatase and (b) rutile (from [50]).

3. TiO_2-based materials (rutile and anatase)

3.1. Introduction

In addition to ZnO, other compounds can be used as a mother matrix. Titanium dioxide TiO_2 is interesting due to many properties and occurs in several forms, such as rutile, anatase and brookite (see the diagrams of the most stable phases in figure 6). Rutile is tetragonal ($a = 4.59$ Å and $c = 2.96$ Å) with a bandgap of 3 eV while the anatase phase also crystallizes in a tetragonal structure ($a = 3.78$ Å and $c = 9.52$ Å) with a bandgap of 3.2 eV [35].

Single-phase TiO_2 thin films, of either rutile or anatase structure, can be prepared on (100)-$SrTiO_3$ substrates by *in situ* PLD [36]. Epitaxial anatase thin films can also be fabricated on lattice-matched (0.2%) (100)-$LaAlO_3$ substrates in the layer-by-layer fashion by laser MBE. X-ray diffraction and transmission electron microscopy show the films grown on (100)-$LaAlO_3$ to exhibit high crystallinity and atomically defined interfaces with an optical bandgap of 3.3 eV at room temperature [37]. As a result, the metastable anatase form of TiO_2, which is difficult to stabilize in bulk, can be grown in the thin film form by the choice of an appropriate lattice-matched substrate. Epitaxial rutile films can also be obtained when using (111)-$SrTiO_3$ substrates [38]. Anatase TiO_2 is a wide bandgap semiconductor with excellent optical transmission in the visible and near-infrared regions, a high refractive index, high dielectric constant ($\varepsilon_R = 105$ at 4.2 K) [39], low tangential loss ($\tan\delta = 10^{-7}$ at 4.2 K) [40] and useful photocatalysis properties [41].

3.2. The growth of Co:TiO_2 thin films

The discovery of room temperature FM, using a combinatorial thin film library of TiO_2 doped with various 3d transition metals by Matsumoto *et al* [8], was the first step in the interest in O-DMS. After this, many Co:TiO_2 films have been reported with various properties that will be discussed in this section.

Most of the films are grown using PLD [42–45] but reactive co-sputtering [47], metal–organic chemical-vapour deposition (MOCVD) [48], oxygen-plasma-assisted molecular beam epitaxy (OPA-MBE) [48–51] and even the sol–gel method [52] have also been employed. As has already been said, anatase/rutile TiO_2 can be synthesized on different substrates and thus various substrates have been utilized, such as α-$Al_2O_3(1\bar{1}02)$ [44], (100)-$SrTiO_3$ [42, 43, 45, 50, 51], (100)-$LaAlO_3$ [42, 45, 50], (100)-Si [47] and SiO_2/Si [48].

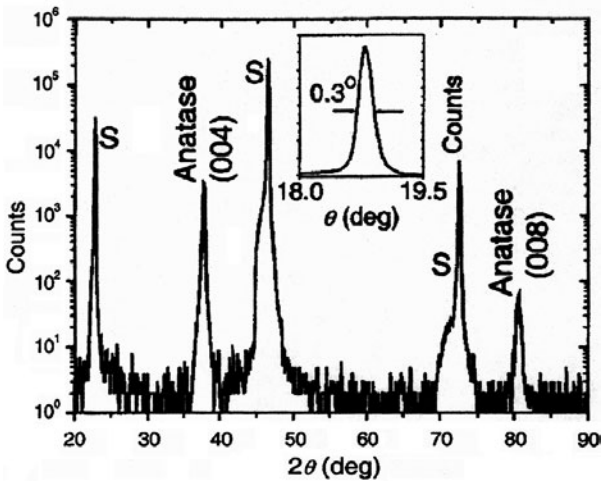

Figure 7. XRD patterns for a $Ti_{0.93}Co_{0.07}O_{2-\delta}$ films on $SrTiO_3$(100). Peaks labelled 'S' correspond to the substrate. The inset shows the rocking curve of the same film (from [42]).

On $SrTiO_3$ substrates, the films are (001)-oriented (figure 7) and the low value of the full width at half-maximum (FWHM) of the rocking curve (0.3°) confirms their high quality (see, for example, the inset of figure 7). While films are grown around 700 °C by PLD, the deposition temperature is close to 550 °C by OPA-MBE [49], 400 °C by MOCVD [48] or 350 °C by sputtering [47] and the deposition pressure is always low ($<10^{-4}$–10^{-5} Torr). This non-dependence of the substrate temperature is confirmed by Chambers *et al* [50] who also show that a slow growth rate results in layer-by-layer growth. Thus, clear typical RHEED oscillations [44, 50] were observed during the growth of TiO_2 (see figure 8). In fact, the growth of Co:TiO_2 is strongly dependent on the oxygen pressure during the deposition [43]. For example, films grown at an oxygen pressure greater than 10^{-5} Torr showed clear streaky RHEED patterns, which suggest two-dimensional (2D) layer-by-layer growth with very smooth surfaces whereas for the films grown at lower oxygen pressure, as the film growth progressed, the patterns turned into three-dimensional (3D) spotty patterns [43]. The rocking curve of the (004) peak for the film grown at 10^{-5} Torr shows a FWHM of 0.66°, which is similar to that reported by Murakami *et al* [37] and as the oxygen pressure decreased down to 10^{-7} Torr, the FWHM increased to 0.86°, indicating that the film grown under low pressure shows a wider mosaic spread.

The lattice mismatch between anatase TiO_2(001) and $SrTiO_3$(001) is 3.1%, assuming a cube-on-cube orientation (i.e. (001)anatase ∥ (001)$SrTiO_3$ and [100]anatase ∥ [100]$SrTiO_3$) [50].

Chambers *et al* claimed that the diffusion of Co (at least up to 10%) is easy in the TiO_2 material [49] when grown on $SrTiO_3$, whereas the solid solution seems to be more limited (2–7%) for films deposited on $LaAlO_3$ [8, 42]. In fact, the out-of-plane lattice parameter (*c* axis on $LaAlO_3$) increases monotonically with increases in Co content following Vergard's law [8] but the intensity of the diffraction peak decreases as the Co content increases, suggesting the presence of matrix disorder for high Co doping [42]. For the case of 2% Co doped films in the as-grown, Co metal clusters of size 20–50 nm were observed. These clusters were seen to dissolve in a TiO_2 matrix after high temperature annealing [42]. For greater concentrations, clusters of Co, whose sizes are approximately 150 nm, were observed [48]. An important

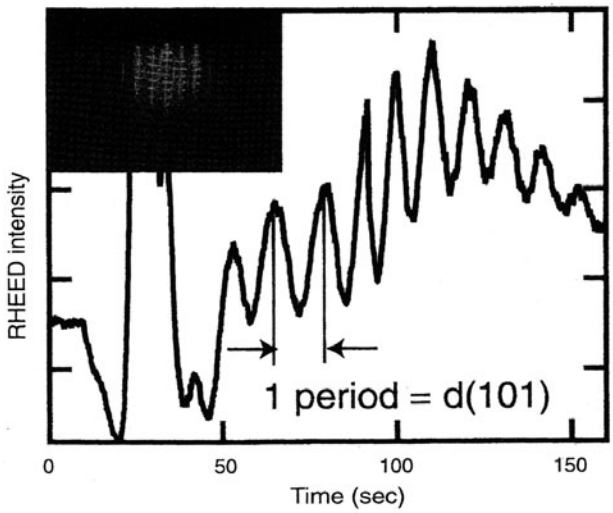

Figure 8. The specular beam intensity in the RHEED pattern versus time during the deposition of TiO_2 on α-Al_2O_3. The inset image is the RHEED pattern of the film (from [44]).

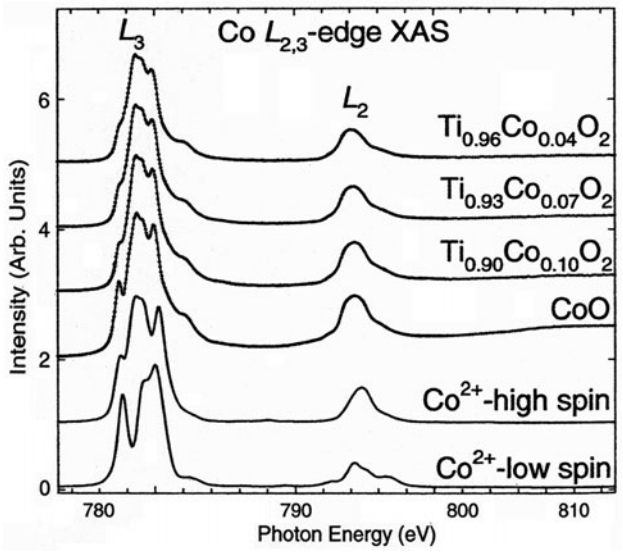

Figure 9. Co $L_{2,3}$-edge XAS spectra of $Ti_{1-x}Co_xO_2$ ($x = 0.04$, 0.07 and 0.1) in comparison with those of CoO and theoretical calculation spectra for high spin Co^{2+} ($3d^7$; $S = 3/2$) and low spin Co^{2+} ($3d^7$; $S = 1/2$) states under O_h symmetry (from [53]).

question arising from the study of the solid solution is on the Co state which is answered by using $L_{2,3}$-edge x-ray absorption spectroscopy (XAS) measurements [50, 51, 53]. The spectra (figure 9) resulting from the Co $2p \rightarrow 3d$ dipole transitions are dominated by the large 2p core–hole spin–orbit coupling energy dividing the spectra into L_3 and L_2 regions. From this, the authors concluded that the ionic ground state of doped Co in $Ti_{1-x}Co_xO_2$ is high spin divalent, i.e. Co^{2+} ($3d^7$; $S = 3/2$) [53], in contrast to previous reports where Co(II) is in a low spin state [44, 49].

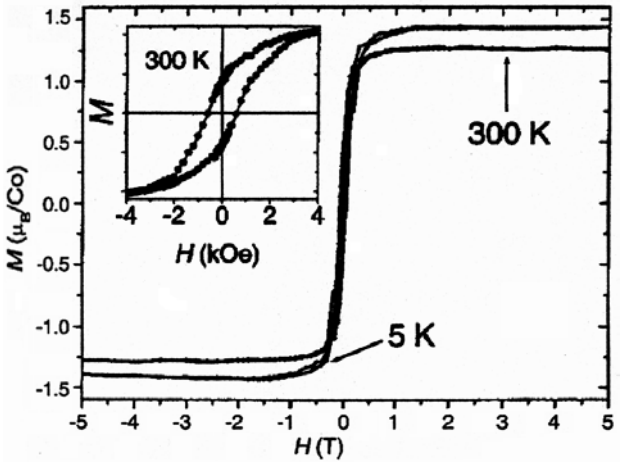

Figure 10. Magnetization (M) as a function of magnetic field (H) for a $Ti_{0.93}Co_{0.07}O_{2-\delta}$ film grown on $SrTiO_3$. The 300 K hysteresis loop is shown in the inset (from [42]).

The distribution of Co inside the TiO_2 matrix is also strongly dependent on the growth process. For example, under certain conditions, highly Co-enriched TiO_2 anatase clusters nucleate on epitaxial TiO_2 anatase grown on (100)-$LaAlO_3$ and, in the most extreme cases, virtually all incident Co segregates to the clusters, yielding a nanoscale ferromagnetic phase that is not ferromagnetic in homogeneous films of the same Co concentration. Chambers *et al* [51] concluded that the nucleation of this phase simultaneously with continuous epitaxial film growth must be carefully monitored in order to avoid drawing false conclusions about the film structure. The Co distribution in the film was also found to depend critically on the way in which the growth was terminated [49]. As an example, when using the MBE process, stopping growth by simultaneously closing the metal source shutters, turning off the oxygen plasma and pumping out the residual oxygen as the sample cooled consistently produced films which were either stoichiometric or substoichiometric in Co. In contrast, terminating the growth by closing the metal shutters and allowing the sample to cool in the oxygen plasma beam consistently resulted in significant Co segregation [49]. Moreover, Kim *et al* [43] suggest that the oxygen vacancies in the anatase TiO_2 films (grown at low oxygen pressure) will help the diffusion of the Co ions, resulting in the formation of nanoclusters. Note that the magnetic properties of Co:TiO_2 films are also found to depend critically on the Co distribution.

3.3. The physical properties of Co:TiO_2 thin films

Many authors have reported FM at room temperature [8, 42, 47] in Co:TiO_2 films independently of the substrate. This is shown by the magnetization versus magnetic field at 300 K (see figure 10) where hysteresis is observed. The SQUID data only showed a Curie temperature greater than 400 K [8, 42, 44, 47, 48, 52]. Using vibrating sample magnetometry, Shinde *et al* [42] found a T_C close to 650 K, suggesting that Co:TiO_2 (low doped films in an as-grown state and 7% doped films after annealing) could be an intrinsic DMS. Note that the Curie temperature of cobalt metal is 1404 K. As the Co content increases, the saturation magnetization abruptly increases and the coercive field markedly decreases, confirming that the magnetic properties of $Ti_{1-x}Co_xO_2$ thin films depend on the critical Co-doping level [48].

Magnetization measurements show that black tinged TiO_2:Co films grown in 1 mTorr oxygen are magnetic while the green tinged films grown at 3 mTorr are non-magnetic. A possible explanation is that at the higher pressures the cobalt surface clusters shown by the TEM are oxidized to form paramagnetic cobalt oxides. The different colours may indicate the different oxidation states of the cobalt. The morphology of the non-magnetic films is currently being investigated by further TEM measurements. The change from magnetic to non-magnetic films with an increase in oxidation was also seen by Chambers *et al* [49–51].

For the saturation magnetic moment per Co atom many values can be found. For example, Matsumoto *et al* [8] find 0.32 μ_B/Co for $Ti_{0.93}Co_{0.07}O_2$ on $LaAlO_3$ and 1 μ_B/Co for $Ti_{0.95}Co_{0.05}O_2$ on α-Al_2O_3 [44]. Park *et al* [47] estimated it to be 0.94 μ_B/Co for $Ti_{1-x}Co_xO_2$ on Si ($x > 0.06$). Similar values were reported by Shinde *et al* [42] (1.4 μ_B/Co for $Ti_{0.93}Co_{0.07}O_2$ grown on both $SrTiO_3$ and $LaAlO_3$) and Chambers *et al* [51] (1.2 μ_B/Co for $Ti_{0.93}Co_{0.07}O_2$ on $LaAlO_3$). The highest value (1.7 μ_B/Co) was measured by Stampe *et al* [45] for $Ti_{0.93}Co_{0.07}O_2$ with an uncertainty of ± 0.4 μ_B/Co on $LaAlO_3$ but not on $SrTiO_3$. They attributed this feature to the strong dependence of the film mosaicity, which results in particular to the twins of the $LaAlO_3$ substrate. These results suggest that the growth conditions, in particular the oxygen pressure, play an important role in the formation of Co clusters and/or the Co:TiO_2 phase and thus lead to a wide range of magnetic moments 0.3–1.7 μ_B/Co. This is confirmed by the study on its dependence versus oxygen pressure [43]. As shown in figure 11, most of the films deposited at a partial pressure of oxygen under 3×10^{-5} Torr had saturation magnetization values close to that of bulk cobalt (1.7 μ_B/Co). Also, the magnetization versus temperature data, shown in the inset of figure 11, shows that FM persists at least up to 750 K. In particular, for the film grown at an oxygen pressure of 10^{-7} Torr, the magnetization does not decrease much with temperature. They explained this dependence of the magnetic properties of the Co:TiO_2 films in terms of the Co nanoclusters [43]. Also, the oxygen vacancies in the anatase TiO_2 films grown at low oxygen pressure will help the diffusion of the Co ions, resulting in the formation of the nanoclusters and, as the number of Co clusters increases, the saturation magnetization will become larger. The remanence and coercivity were found to be close to 20% and around 125 Oe, respectively, for Co:TiO_2 ($x = 0.05$) [51]. Finally, by recording longitudinal Kerr loops as a function of angle between the magnetic field direction and the [100] direction of $SrTiO_3$, no significant in-plane magnetic anisotropy was found [49].

By growing epitaxial thin films of $Ti_{1-x}Co_xO_2$, with $x = 0.01$ and 0.07, by PLD in both the anatase and rutile forms on single-crystal substrates of $LaAlO_3$, $SrTiO_3$ and Al_2O_3, Stampe *et al* [46] found ferromagnetism at room temperature with a magnetic moment of $\sim$1.7 μ_B/Co in the anatase phase and $\sim$0.6 μ_B/Co in the rutile phase. Detailed transmission electron microscopy measurements show a variation in the cobalt distribution in these materials that corresponds to the different magnetic moments. The cobalt does not appear to enter the anatase phase of TiO_2, but rather forms crystallites of cobalt metal on the surface of the anatase films. Such Co metal clusters are confirmed by several groups [43].

All films show semiconducting or insulating behaviour [8, 45]. Moreover, in the case of a $LaAlO_3$ substrate, the thicker film (1200 nm) shows a small resistivity minimum at $\approx$150 K, while the resistivity for the thinner Co:TiO_2 film (200 nm) increases monotonically with decreasing temperature. This was found to be a general feature, although there is no definitive 'crossover' thickness for which the resistivity changed behaviour. The reported room temperature resistivity values are about 0.1–1 Ω cm for $Ti_{0.94}Co_{0.06}O_2$ on $LaAlO_3$ [8] and around six times larger than the $Ti_{0.93}Co_{0.07}O_2$ films grown on $SrTiO_3$ [45]. There is no consistent change in room temperature resistivity with dopant concentration, even though a large effect would be expected with the addition of these large quantities of metallic dopants [45]. Finally, the Hall effect measurements show n-type conduction with a carrier

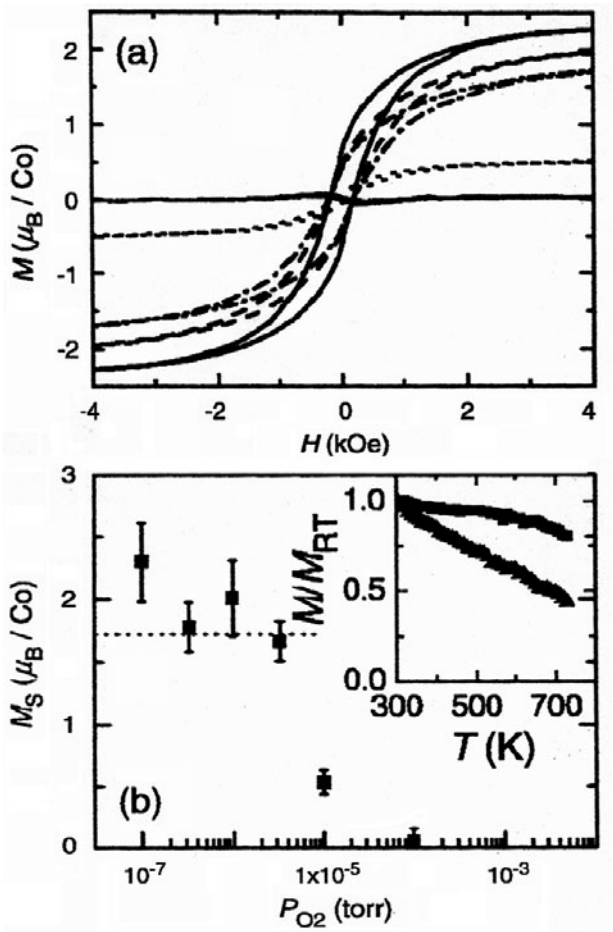

Figure 11. (a) Magnetization versus magnetic field curves at 300 K for the $Ti_{0.96}Co_{0.04}O_2$ thin films under various partial oxygen pressures. The data for the films grown at 10^{-7}, 3.3×10^{-7}, 10^{-6}, 3.3×10^{-6}, 10^{-5} and 10^{-4} Torr are shown as the full, broken, chain, dotted and short-dotted curves, respectively. (b) Dependence of the saturation magnetization on the partial pressure of oxygen. The dotted line corresponds to the bulk cobalt metal value. The inset shows the temperature dependence of the normalized magnetization for the films grown at a partial pressure of 10^{-7} Torr (squares) and 10^{-5} Torr (triangles) (from [43]).

concentration at 300 K of around 1.4×10^{18} cm^{-3} for $Ti_{0.99}Co_{0.01}O_2$ [42] and 10^{18} cm^{-3} for $Ti_{0.93}Co_{0.07}O_2$ [8]. According to Matsumoto *et al* [8] it is scarcely dependent on the Co doping level.

Another interesting feature of these DMS is the magnetoresistance (MR is defined as $[R(H) - R(0)]/R(0)$) effect at low temperature. While the MR under a 8 T magnetic field in an undoped film at 3 K is 6%, it is 23% in $Ti_{0.99}Co_{0.01}O_{2-\delta}$ and 40% in $Ti_{0.98}Co_{0.02}O_{2-\delta}$ [42]. For higher concentrations, >2%, the MR was seen to be the same as that at 2%. A similar value of 60% at 2 K was reported for $Ti_{0.93}Co_{0.07}O_2$ (when the field is applied perpendicular to the surface plane) [8]. For higher Co content, Shinde *et al* [42] attributed the low temperature high MR to Zeeman splitting of the band states through their coupling to Co spins.

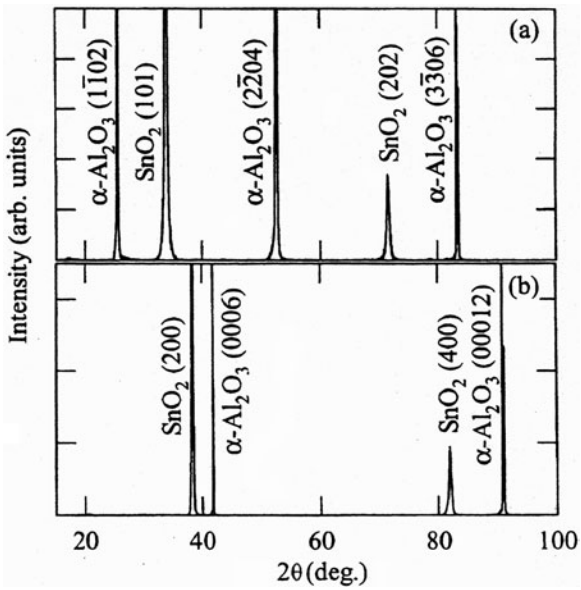

Figure 12. XRD patterns of $Sn_{0.95}Mn_{0.05}O_2$ films on (a) R-sapphire and (b) C-sapphire substrates. Note the difference in the orientation of the films (from [54]).

4. Some other host matrix: rutile and perovskite types

Other host matrices have been used to search for new DMS systems such as rutile-type SnO_2 [54–56], Cu_2O [57], $La_{1-x}Sr_xTiO_3$ [58], (Ba, Sr)TiO_3 and $KTaO_3$ [59, 60]. The first three samples are thin films grown by using the PLD technique whereas the latter two cases ((Ba, Sr)TiO_3 and $KTaO_3$) are single crystal.

4.1. Rutile-type structures: SnO_2

Based on the properties of TiO_2-based thin films, some researchers have looked at other matrices having the same rutile-type structure. SnO_2. which also has interesting optical and electrical properties, is one of such an example. Moreover, SnO_2 has an n-type conduction [61] which is potentially interesting for spintronic devices. In this case, the films are grown by laser ablation on sapphire substrates with a $(1\bar{1}02)$ [54–56] or (0001) orientation (respectively called R-cut and C-cut). Mn [54, 55] or Co [56] have been used as a dopant in the rutile matrix. For Co:SnO_2 samples, good XRD patterns were obtained even for films with cobalt concentrations as high as 30% (i.e. $x = 0.3$), but a decrease in the XRD peak intensity was encountered for further increases in Co content (i.e. for $x > 0.3$) [56]. Kimura *et al* [54, 55] have shown that the Mn ions are also soluble in SnO_2 films up to 30% moles, which is higher than the thermal equilibrium, most probably due to the non-equilibrium growth process of PLD. As the Mn content increases, changes in lattice constants are observed, confirming that the 0.0 Mn ions enter the SnO_2 structure. Figure 12 depicts the resulting XRD patterns of $Sn_{0.95}Mn_{0.05}O_2$ thin films grown on sapphire substrates. Three remarks should be pointed out. Firstly, there is no impurity phase other than the rutile phase. Secondly, the film is well oriented, which is confirmed by the value of the FWHM being less than 0.5° for $Sn_{0.95}Mn_{0.05}O_2$. Note that for $Sn_{0.95}Mn_{0.05}O_2$ the value of FWHM decreases as x decreases whereas no such changes were observed for $Sn_{1-x}Co_xO_2$ films (not shown). Thirdly, the orientation of the film with

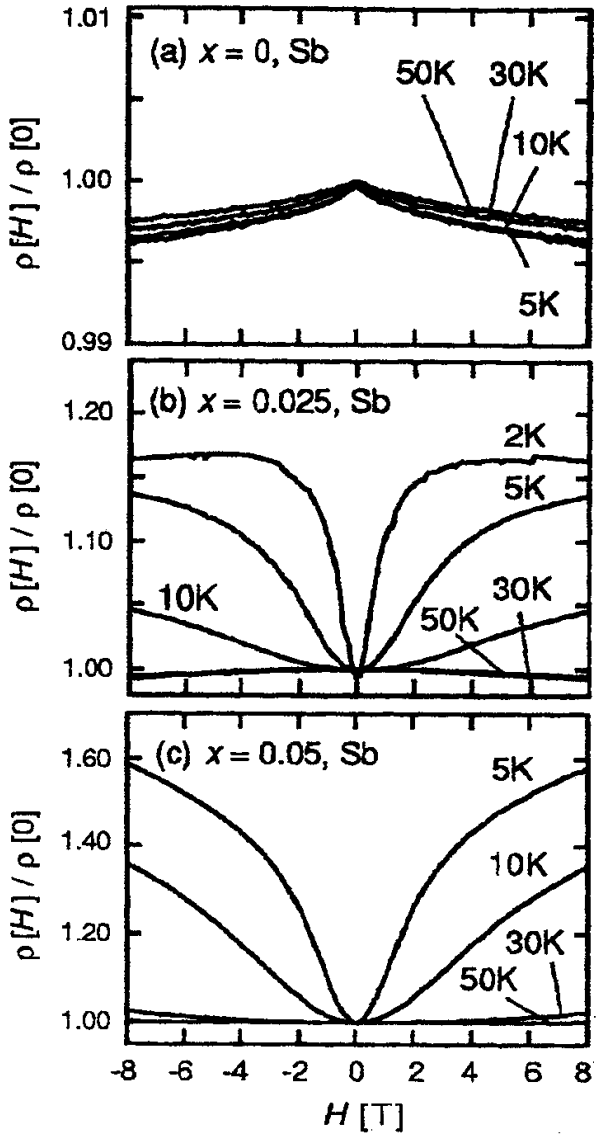

Figure 13. Isothermal MR at various temperatures for (a) SnO_2:Sb, (b) $Sn_{0.975}Mn_{0.025}O_2$:Sb and (c) $Sn_{0.95}Mn_{0.05}O_2$:Sb films deposited on R-Al_2O_3. The magnetic field is applied normal to the film surface (from [55]).

respect to the substrate plane is different on both substrates: (101) on R-sapphire and (100) on C-sapphire substrates. Surprisingly, the Mn-doped films do not exhibit FM. In fact, the film is almost paramagnetic and the resistivity rapidly increases with temperature below 50 K (at 300 K, the resistivity is close to 0.5 Ω cm) while the Co-doped films ($Sn_{0.95}Co_{0.05}O_{2-\delta}$) have a Curie temperature close to 650 K. Surprisingly these films (5% co-doping) show a giant magnetic moment [56] of $7 \pm 0.5\ \mu_B$/Co. The Sb doping into Mn-doped SnO_2 results in metallic conductivity [54, 55] with n-type carriers of 6.7×10^{20} cm^{-3}. Figure 13 shows the isothermal MR for $Sn_{1-x}Mn_xO_2$:Sb films. The MR ratio at 2 K calculated using the formula

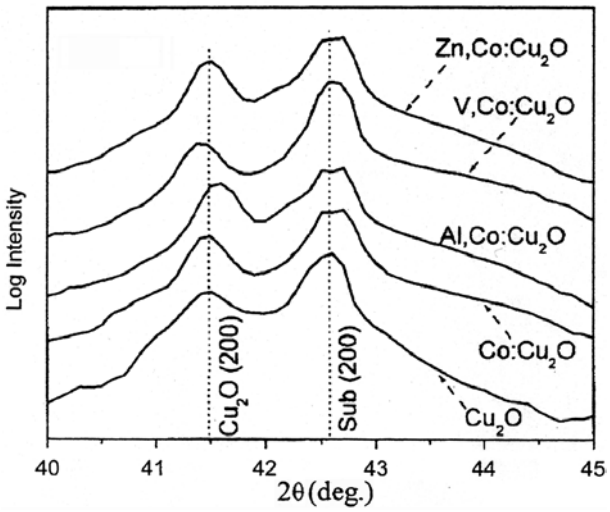

Figure 14. XRD pattern of Co-doped Cu_2O films on MgO with and without Al, Zn and V dopants. The patterns are shifted along the y axis for clarity (from [57]).

MR(%) $= 100[\rho(H) - \rho(0)]/\rho(0)$ is as high as 15% for $x = 0.05$ and reaches up to 60% for $x = 0.15$ in 8 T at 5 K.

4.2. Perovskite-type structures: $ATiO_3$ (A = Ba, Sr, La)

The implantation at elevated temperatures of Co [59] or Mn [60] was made into single-crystal $BaTiO_3$(K), $SrTiO_3$ or $KTaO_3$(Ca). Following annealing at 700 °C, the implantations of Mn [60] or Co produced ferromagnetic behaviour over a broad range of cobalt concentrations [59]. For $BaTiO_3$, this process produced magnetic ordering temperatures above 300 K with coercivities <=70 Oe in the cases of Co and Mn. The magnetization–temperature plots showed a non-Brillouin-shaped curve in the case of Mn and a near-linear decrease of magnetization with increasing temperature in the case of Co implantation. No secondary phases were detected within the sensitivity of high-resolution x-ray diffraction and similar results were observed for both $SrTiO_3$ and $KTaO_3$ with the exception that, at high Mn concentrations (∼5 at.%), the $SrTiO_3$ was no longer ferromagnetic. The substitution of Co into a perovskite structure was also investigated in the case of $La_{1-x}Sr_xTiO_3$ [58]. They claimed that the system has the characteristics of an intrinsic DMS (metal) at low concentrations (<2%), but develops inhomogeneity at higher cobalt concentrations, with a ferromagnetic transition near 450 K. The films range from being opaque metallic to transparent semiconducting, depending on the oxygen pressure during growth.

4.3. Other structures: the example of Cu_2O

Cu_2O is an interesting candidate because it is a p-type semiconducting oxide with a cubic structure ($a = 4.27$ Å) and a bandgap of 2.0 eV. Kale *et al* [57] synthesized a series of films with the formula $Co_{0.05}R_{0.005}Cu_{0.945}O$ (where R = Al, V and Zn) on (001)MgO substrates by PLD. The films showed pure phase character under the chosen optimum growth conditions (substrate temperature: 700 °C and oxygen partial pressure of 10^{-3} Torr) as seen from the corresponding XRD patterns (figure 14) in the range 40°–45°. It is useful to mention here that

high quality Cu_2O films could also be grown on R-plane sapphire substrates, but with (110) orientation. The optical bandgap of the film is about 2.05 eV. A spin-glass-like behaviour was observed in Co-doped films without co-doping and some particular features are observed at 170 and 250 K. However, a clear ferromagnetic signal at room temperature with coercivity of about 50 Oe was found only in the case of Co:Cu_2O films co-doped with Al. The observed moment per Co calculated close to 0.44 μ_B/Co ruled out the possibility of pure Co metal clusters since it is rather small compared to Co (1.7 μ_B/Co) or Co nanoclusters (2.1 μ_B/Co). The room temperature resistivity for undoped film is 225 Ω cm and it increases to 512 Ω cm with Co doping. Upon co-doping with Al, V and Zn, the resistivity changes to 500, 1800 and 46 Ω cm, respectively.

5. Conclusion

The interesting room temperature FM, in many diluted magnetic semiconductor oxide systems (O-DMS), has opened up a route for spintronic devices. Based on theoretical calculations [7], the ZnO compound has been extensively studied as a host matrix for being doped essentially with Co. Most of the films obtained exhibit FM above room temperature, as expected from the theory, but some authors claimed that it arises from Co clusters. Several dopants have also been utilized, such as Mn or V. Theories predicted FM for these materials. However, some authors did not find any Curie temperature in the case of Mn. The doping of various matrices, such as TiO_2, or SnO_2, has also been studied. In a similar way to ZnO, the Co and Mn doping was explored leading to controversial results, especially in the case of Co doping. A solution to dismiss this problem is to use an element that can form clusters and a good example was obtained with V [16].

In fact, a clear picture of the origin of magnetism in O-DMS has not been obtained. Up to now, it seems that the growth process, including the growth conditions (oxygen pressure and temperature) but also the growth technique (PLD versus molecular beam epitaxy, for example), have a strong influence on the properties of the films. This has been clearly shown in the case of TiO_2 [51].

Despite all of these questions that have opened a large debate, it seems that there is an intrinsic mechanism that can lead to FM close to room temperature. Additional work is needed to clarify the exact origin of the FM which will require a more precise control of the dopant inside the mother structures and careful structural/microstructural analysis.

Acknowledgments

We acknowledge Satish Ogale, Sanjay Shinde and Ram Choudhary (Center for Superconductivity Research of the University of Maryland) for their careful reading of the manuscript and helpful comments.

We also thank M Morin for helping with the preparation of the manuscript and H H Nguyen for discussions. Financial support from the CNRS and the 'Conseil Regional de Basse Normandie' is greatly acknowledged.

References

[1] Wolf S A, Awschalom D D, Buhrman R A, Daughton J M, von Molnar S, Roukes M L, Chtchelkanova A Y and Treger D M 2001 *Science* **294** 1488
[2] Furdyna J K 1998 *J. Appl. Phys.* **64** R29
[3] Ohno H 1998 *Science* **281** 951
[4] Sato K and Katayama-Yoshida H 2000 *Japan. J. Appl. Phys.* **40** L485

[5] Akinaga H, Manago T and Shirai M 2000 *Japan. J. Appl. Phys.* **39** L1118
Medvedkin G A, Ishibashi T, Nishi T, Hayata K, Hasegawa Y and Sato K 2000 *Japan. J. Appl. Phys.* **39** L949
[6] See Dietl T, Ohno H, Matsukura F, Cibert J and Ferrand D 2000 *Science* **287** 1019
[7] Sato K and Katayama-Yoshida H 2000 *Japan. J. Appl. Phys.* **39** L555
[8] Matsumoto Y, Murakami M, Shono T, Hasegawa T, Fukumara T, Kawasaki M, Ahmet P, Chikyow T, Koshihara S Y and Koinuma H 2001 *Science* **291** 854
[9] Wyckoff R W G 1986 *Crystal Structures* 2nd edn (New York: Wiley)
[10] Joseph M, Tabata H and Kawai T 1999 *Japan. J. Appl. Phys.* **38** L1205
[11] Muthukumar S, Zhong J, Chen Y, Lu Y and Siegrist T 2003 *Appl. Phys. Lett.* **82** 742
[12] Kim C, Leem S J, Robinson I K, Park W I, Kim D H and Yi G C 2002 *Phys. Rev.* B **66** 113404
[13] Wakano T, Fujimura N, Morinaga Y, Abe N, Ashida A and Ito T 2001 *Physica* E **10** 260
[14] Ueda K, Tabata H and Kawai T 2001 *Appl. Phys. Lett.* **79** 988
[15] Yoo Y Z, Jin Z W, Chikyow T, Fukumara T, Kawasaki M and Koinuma H 2002 *Appl. Phys. Lett.* **81** 3798
[16] Saeki H, Tabata H and Kawai T 2001 *Solid State Commun.* **120** 439
[17] Fukumura T, Jin Z, Ohtomo A and Koinuma H 1999 *Appl. Phys. Lett.* **75** 3366
[18] Cheng X M and Chien C L 2003 *J. Appl. Phys.* **93** 7876
[19] Kim D S, Kim H M, Yuldashev S U, Lee S J, Kang T W and Kim D Y 2003 *J. Korean Phys. Soc.* **42** S333
[20] Tiwari A, Jin C, Kvit A, Kumar D, Muth J F and Narayan J 2002 *Solid State Commun.* **121** 371
[21] Jung S W, An S J, Yi G C, Jung C U, Lee S I and Cho S 2002 *Appl. Phys. Lett.* **80** 4561
[22] Jin Z *et al* 2001 *Appl. Phys. Lett.* **78** 3824
[23] Han S J, Song J W, Yang C H, Park S H, Park J H, Jeong Y H and Rhie K W 2002 *Appl. Phys. Lett.* **81** 4212
[24] Prellier W, Fouchet A, Mercey B, Simon Ch and Raveau B 2003 *Appl. Phys. Lett.* **82** 3490
[25] Rode K, Anane A, Mattana R, Contour J P, Durand O and LeBourgeois R 2003 *J. Appl. Phys.* **93** 7676
[26] Kim J H, Kim H, Kim D, Ihm Y E and Choo W K 2003 *Physica* B **327** 304
[27] Kim J H, Choo W K, Kim H, Kim D and Ihm Y E 2003 *J. Korean Phys. Soc.* **42** S258
[28] Yoo Y-Z, Fukumura T, Jin Z, Hasegawa K, Kawasaki M, Ahmet P, Chikyow T and Koinuma H 2001 *J. Appl. Phys.* **90** 4246
[29] Lim S W, Hwang S K and Myoung J M 2003 *Solid State Commun.* **125** 231
[30] Kim J H, Kim H, Kim D, Ihm Y E and Choo W K 2002 *J. Appl. Phys.* **92** 6066
[31] Lee H J, Jeong S Y, Cho C R and Park C H 2002 *Appl. Phys. Lett.* **81** 4020
[32] Kim K J and Park Y R 2002 *Appl. Phys. Lett.* **81** 1420
[33] Cho Y M, Choo W K, Kim H, Kim D and Ihm Y E 2002 *Appl. Phys. Lett.* **80** 3358
[34] Ando K, Saito H, Jin Z, Fukumura T, Kawasaki M, Matsumoto Y and Koinuma H 2001 *Appl. Phys. Lett.* **78** 2700
[35] Tang H, Berger H, Schmid P E and Levy F 1994 *Solid State Commun.* **92** 267
[36] Hsieh C C, Wu K H, Juang J Y, Uen T M, Lin J-Y and Gou Y S 2002 *J. Appl. Phys.* **92** 2518
[37] Murakami M, Matsumoto Y, Nakajima K, Makino T, Segawa Y, Chikyow T, Ahmet P, Kawasaki M and Koinuma H 2001 *Appl. Phys. Lett.* **78** 2664
[38] Kennedy R J and Stampe P A 2003 *J. Cryst. Growth* **252** 333
[39] Parker N J, Kharel P, Powell J R, Smith P A, Evans P D and Porch A 1999 *IEEE Trans. Appl. Supercond.* **9** 1928
[40] Zuccaro C, Ghosh I, Urban K, Klein N, Penn S and Alford N M 1997 *IEEE Trans. Appl. Supercond.* **7** 3715
[41] Augustynski J 1993 *J. Electronchim. Acta* **38** 43
[42] Shinde S R *et al* 2003 *Phys. Rev.* B **67** 115211
[43] Kim D H *et al* 2002 *Appl. Phys. Lett.* **81** 2421
[44] Matsumoto Y, Takahashi R, Murakami M, Koida T, Fan X J, Hasegawa T, Fukumura T, Kawasaki M, Koshihara S Y and Koinuma H 2001 *Japan. J. Appl. Phys.* **40** L1204
[45] Stampe P A, Kennedy R J, Xin Y and Parker J S 2002 *J. Appl. Phys.* **92** 7114
[46] Stampe P A, Kennedy R J, Xin Y and Parker J S 2003 *J. Appl. Phys.* **93** 7864
[47] Park W K, Ortega-Hertogs R J, Moodera J S, Punnoose A and Seehra M S 2002 *J. Appl. Phys.* **91** 8093
[48] Seong N J, Yoon S G and Cho C R 2002 *Appl. Phys. Lett.* **81** 4209
[49] Chambers S A *et al* 2001 *Appl. Phys. Lett.* **79** 3467
[50] Chambers S A, Wang C M, Thevuthasan S, Droubay T, McCready D E, Lea A S, Shutthababdan V and Windisch C F Jr 2002 *Thin Solid Films* **418** 197
[51] Chambers S A, Droubay T, Wang C M, Lea A S, Farrow R F C, Folks L, Deline V and Anders S 2003 *Appl. Phys. Lett.* **82** 1257
[52] Soo Y L, Kioseoglou G, Kim S, Kao Y H, Sujatha Devi P, Parise J, Gambino R J and Gouma P I 2002 *Appl. Phys. Lett.* **81** 655

[53] Kim J Y *et al* 2003 *Phys. Rev. Lett.* **90** 017401
[54] Kimura H, Fukumura T, Koinuma H and Kawasaki M 2001 *Physica* E **10** 265
[55] Kimura H, Fukumura T, Kawasaki M, Inabe K, Hasegawa T and Koinuma H 2002 *Appl. Phys. Lett.* **80** 94
[56] Ogale S B *et al* 2003 *Phys. Rev. Lett.* **91** 077205
[57] Kale S N, Ogale S B, Shinde S R, Sahasrabuddhe M, Kulkarni V N, Greene R L and Venkatesan T 2003 *Appl. Phys. Lett.* **82** 2100
[58] Zhao Y G *et al* 2002 *Preprint* cond-mat/0209267
[59] Lee J S, Khim Z G, Park Y D, Norton D P, Budai J D, Noatner L A, Pearton S J and Wilson R G 2003 *Electrochem. Solid State Lett.* **6** J1
[60] Norton D P, Theodoropoulou N A, Hebard A F, Budai J D, Boatner L A, Pearton S J and Wilson R G 2003 *Electrochem. Solid State Lett.* **6** G19
[61] Kilic C and Zunger A 2002 *Phys. Rev. Lett.* **88** 095501